ISSN 1070-4280, Russian Journal of Organic Chemistry, 2022, Vol. 58, No. 1, pp. 144–151. © Pleiades Publishing, Ltd., 2022.

Magnetic Nanoparticle-Supported Basic Ionic Liquid: A Reusable Phase-Transfer Catalyst for Knoevenagel Condensation in Aqueous Medium

M. Fallah-Mehrjardi[a],*, R. Behjatmanesh-Ardakani[a], and S. Saidian[b]

[a] *Department of Chemistry, Payame Noor University, Tehran, 19395-4697 Iran*

[b] *Department of Basic Sciences and General Courses, Faculty of Economics and Management, Khorramshahr University of Marine Science and Technology, Khorramshahr, 64199-34619 Iran*

**e-mail: fallah.mehrjerdi@pnu.ac.ir*

Received April 24, 2021; revised May 19, 2021; accepted May 22, 2021

Abstract—This study addressed the preparation and characterization of polyethylene glycol-substituted 1-methylimidazolium hydroxide supported on magnetic nanoparticles (MNP@PEG-ImOH) by FESEM, FT-IR, EDAX, TEM, TGA, VSM, and XRD techniques. The catalytic activity of MNP@PEG-ImOH has been examined in Knoevenagel condensation between active methylene compounds and aromatic aldehydes in aqueous medium at room temperature. Numerous benefits of the catalytic system, such as higher yields of the products, shorter reaction time, reusability and recyclability of the catalyst, simplified work-up, and more acceptable reaction conditions, have been demonstrated. It is possible to easily isolate the catalyst from the reaction mixture by an external magnet and reapply it in the consequent reactions with no remarkable loss of activity.

Keywords: green synthesis, Knoevenagel condensation, supported ionic liquid, phase-transfer catalyst

DOI: 10.1134/S1070428022010201

INTRODUCTION

Since twenty years ago, researchers developed the supported ionic liquid phase (SILP) technology as one of the new procedures for immobilizing homogeneous ionic liquids in catalysis [1]. Therefore, they introduced numerous techniques for immobilizing the ionic liquids on a solid support like carbon nanotubes (CNTs) [2], mesoporous silica [3], amorphous silica [4], nano-silica [5], polymers [6], as well as graphene oxide (GO) [7]. As a result of multiple functional caveats, like catalyst recovery and product isolation, it would be hard to widely utilize homogeneous ILs and thus supported ionic liquids (SILs) could eliminate the mentioned shortcomings [8]. Therefore, experts in the field have largely employed SILs in organic syntheses because isolation of heterogeneous catalysts from the reaction mixture would be highly simplified and thus they could be re-utilized in the subsequent reactions [9–11].

Magnetic nanoparticles are largely applied in organic syntheses as catalyst supports and catalysts because of their large surface area-to-volume ratio, biocompatibility, lower costs, simple synthesis and functionalization, as well as easy separation using an external magnet [12]. Hence, experts in the field commonly employ MNPs for the immobilization of homogeneous ionic liquids. Moreover, nanomagnetic SILs incorporate the benefits of heterogeneous catalysts, ionic liquids, as well as nano-supports, such as high efficiency, simple transportation, recycling, and separation, and higher designability [13–15].

An appropriate alternative for replacing traditional catalytic systems, which create numerous detrimental by-products, has been proposed to be presentation of mild and green processes with the use of phase-transfer catalysts (PTCs) [16]. Since the majority of organic reactants and substrates are poorly soluble in water, it is possible to eliminate this disadvantage with the use of PTCs. However, a major concern when applying homogeneous PTCs is the recovery of the catalyst from the reaction mixture. An easy solution is PTC immobilization on an insoluble support. The separation of products and the retrieval of catalysts are simplified by a heterogeneous catalyst [17–20].

Scheme 1.

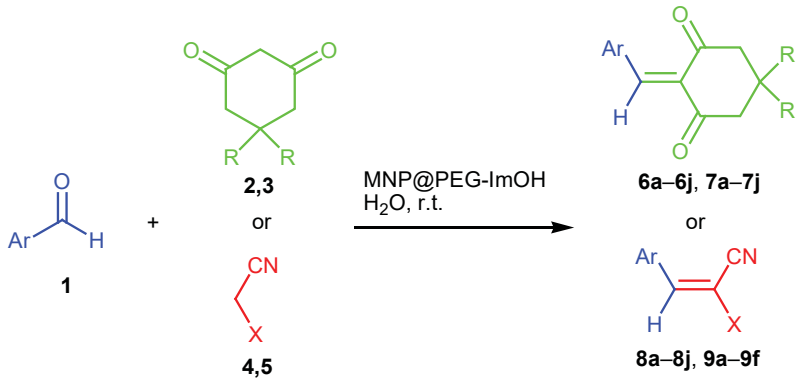

For Ar, X, and R, see Table 1.

A prominent reaction to form the carbon–carbon bond in organic syntheses is the Knoevenagel condensation of an aldehyde with an active methylene compound containing two electron-withdrawing groups [21–25]. The Knoevenagel reaction has often been utilized to synthesize carbocyclic and heterocyclic compounds, pharmaceutically significant organic compounds, as well as fine chemicals [26–30]. The present study reports the synthesis and characterization of a basic ionic liquid supported on MNPs and the respective catalytic application in the Knoevenagel condensation of diverse aromatic aldehydes with active methylene compounds, including dimedone, cyclohexane-1,3-dione, malononitrile, and ethyl cyanoacetate, in water at room temperature (Scheme 1).

RESULTS AND DISCUSSION

Scheme 2 represents the general synthetic route to obtain the basic ionic liquid supported on MNPs. The MNP@PEG NPs catalyst was prepared according to the reported method [31]. Thionyl chloride and pyridine were used to replace the hydroxy groups on the PEG surface with chlorine. The nucleophilic substitution reaction of MNP@PEG-Cl with 1-methylimidazole provided the supported ionic liquid. Finally, a mixture of the obtained nanocomposite and sodium hydroxide in water was stirred at room temperature, and nanomagnetic basic PTC was created.

A number of physicochemical characterization techniques like FT-IR, FESEM, TEM, EDAX, TGA, VSM, and XRD were utilized for probing the structure of the organic–inorganic nanocomposite. Figure 1 compares the FT-IR spectra of MNP@PEG-ImOH, Fe_3O_4@SiO_2, and Fe_3O_4. For all samples, the low-frequency absorption band at ~580 cm^{-1} can be assigned to Fe–O, and a broad band at 3200 to 3600 cm^{-1} was ascribed to vibrations of the surface OH groups. It is notable that the FT-IR spectrum of Fe_3O_4@SiO_2 showed three additional absorption bands at about 1080, 980, and 460 cm^{-1}, which were associated with Si–O–Si asymmetric stretching, symmetric stretching, and bending vibrations, respectively. These peaks confirmed that the surface of Fe_3O_4 magnetic NPs was coated with silica. The immobilization of the ionic liquid on the Fe_3O_4@SiO_2 surface was supported by C–H stretching absorption bands at 2900 to 2950 cm^{-1}, overlapping O–H stretching bands at 2800 to 3600 cm^{-1}, and C–H bending bands at 1400 to 1500 cm^{-1}. Furthermore, absorption bands in the region 1550–1650 cm^{-1} were attributed to imidazole ring stretching and imidazole C=N bending vibrations.

Considering the TEM and FESEM images of the catalyst, a somewhat spherical shape was observed for NPs with diameters of 24 to 143 nm. In addition, the core–shell structure with dark and brighter dots relative to the Fe_3O_4 core and organic part of the catalyst, respectively, was observed in the TEM image (Fig. 2).

As demonstrated in Fig. 3, the EDAX pattern of the catalyst verified the presence of fundamental elements like oxygen (28.4 wt %), iron (51.9 wt %), silicon (5.4 wt %), nitrogen (2.7 wt %), and carbon (11.5 wt %).

The X-ray diffraction patterns of MNP@PEG-ImOH catalyst and Fe_3O_4 magnetic NPs were recorded in the 2θ range from 0 to 80° (Fig. 4). It can be seen that the positions and intensity of the diffraction peaks at 2θ = 30.25°, 35.63°, 43.22°, 53.76°, 57.27°, and 62.88° are perfectly consistent with the pattern for Fe_3O_4 nanoparticles with six peaks at 2θ = 30.31°, 35.69°, 43.32°, 53.81°, 57.26°, and 62.92°.

Scheme 2.

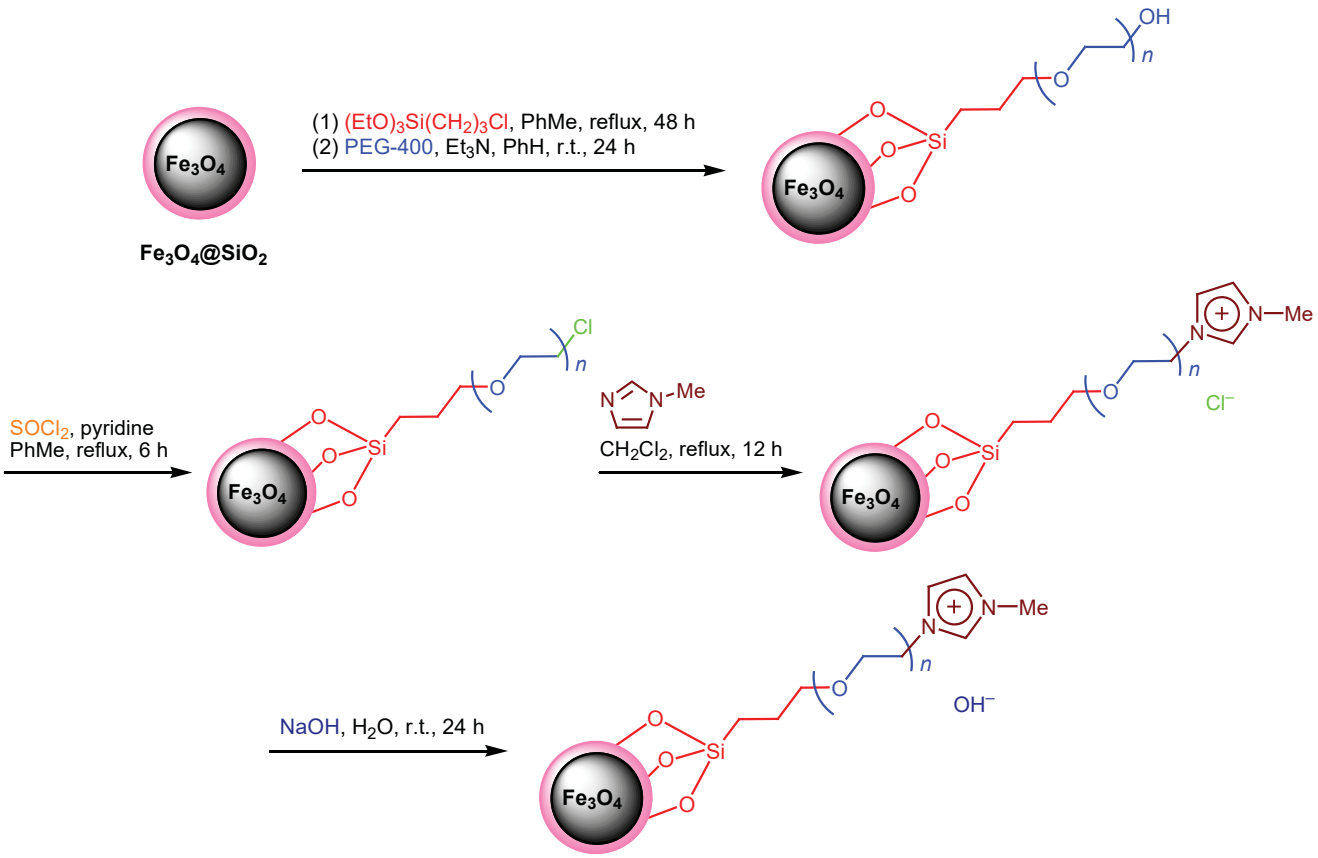

Thermal gravimetric analysis was used to survey the thermal stability of the catalyst. Two distinctive steps of weight loss were observed (Fig. 5). As seen in Fig. 5, the first weight loss below 200°C is due to elimination of physisorbed water molecules. The second weight loss at ~380°C results from thermal crystal phase transformation from Fe_3O_4 to γ-Fe_2O_3 [32] and/or decomposition of the organic materials in MNP@PEG-ImOH.

The magnetic properties of the catalyst were examined at room temperature (Fig. 6). Saturation magnetization values of 58, 43, and 24 emu/g were obtained for Fe_3O_4, Fe_3O_4@SiO_2, and MNP@PEG-ImOH, respectively. It was found that reduction of the

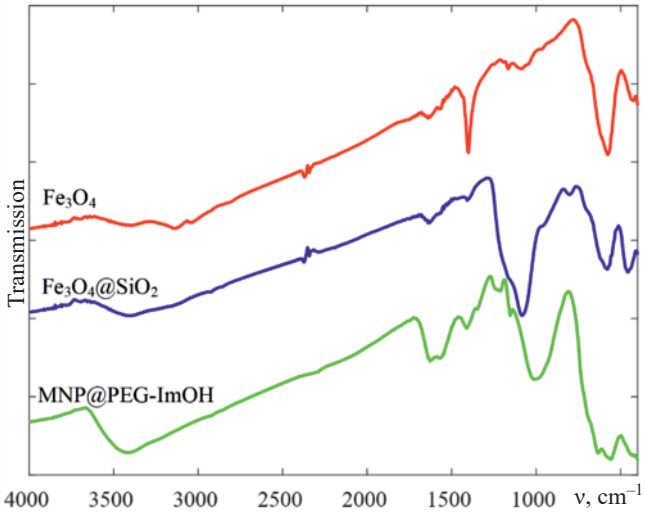

Fig. 1. FT-IR spectra of MNP@PEG-ImOH, Fe_3O_4@SiO_2, and Fe_3O_4 NPs.

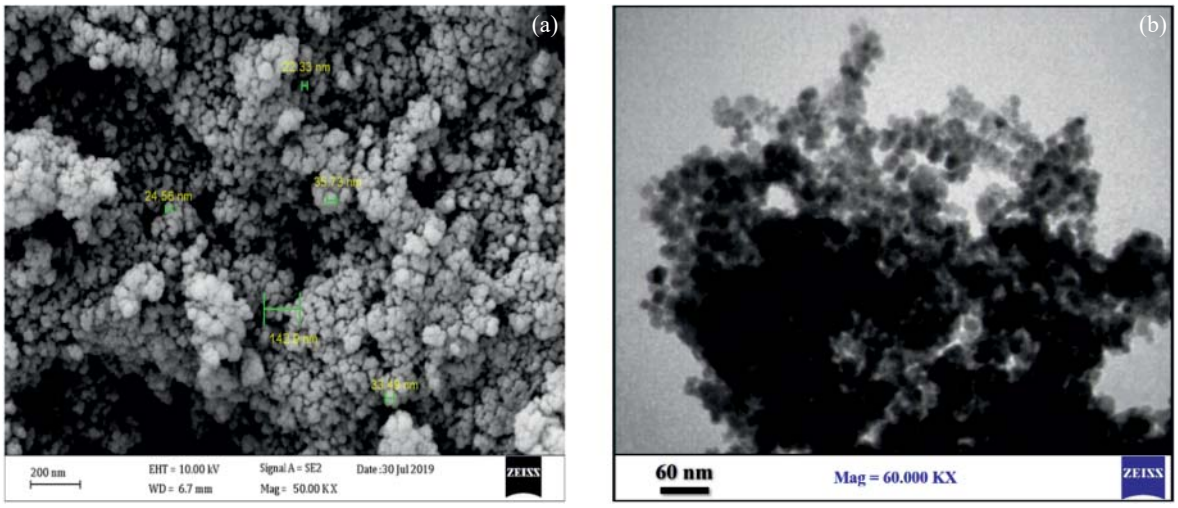

Fig. 2. (a) FESEM and (b) TEM images of MNP@PEG-ImOH.

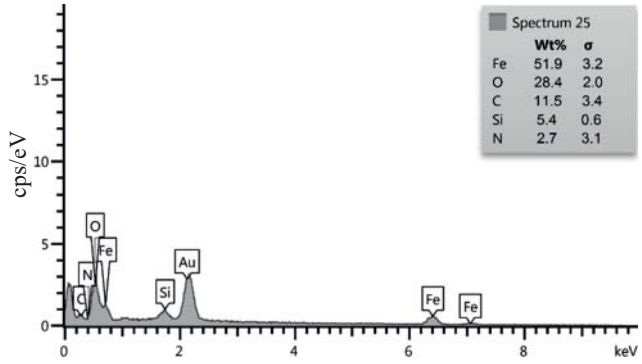

Fig. 3. EDAX pattern of MNP@PEG-ImOH.

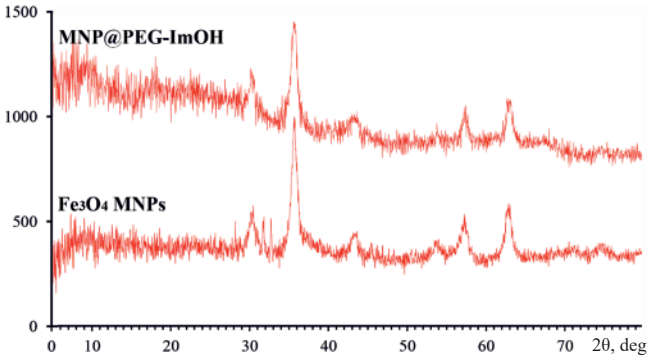

Fig. 4. XRD patterns of MNP@PEG-ImOH and Fe_3O_4 NPs.

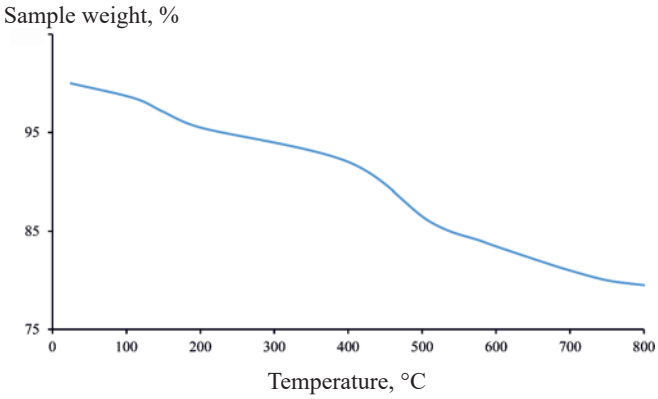

Fig. 5. TGA curve of MNP@PEG-ImOH.

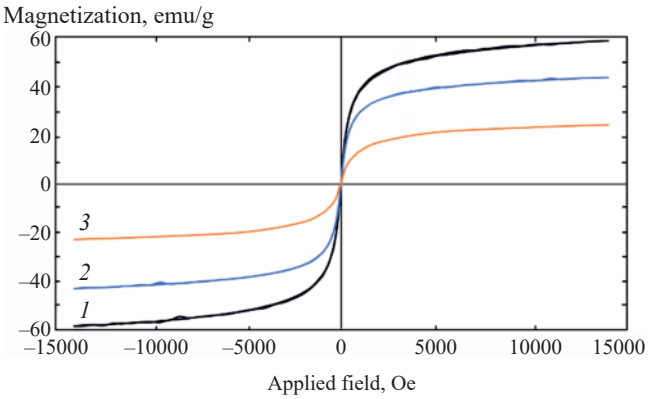

Fig. 6. Magnetization curves of (*1*) Fe_3O_4, (*2*) Fe_3O_4@SiO_2, and (*3*) MNP@PEG-ImOH.

catalyst magnetization results from coating of magnetic NPs with nonmagnetic moieties (imidazolium ring, linker, SiO_2 shell, and PEG chain).

After thorough characterization, the catalytic activity of MNP@PEG-ImOH as a phase-transfer catalyst was assessed in the Knoevenagel condensation. To optimize the conditions, a model reaction of benzaldehyde (1 mmol) and malononitrile (1 mmol) using MNP@PEG-ImOH in water (3 mL) was run at room temperature. Based on TLC data, the most acceptable output was observed when applying 0.02 g of the magnetic nanocomposite (Table 1). Under the optimal conditions, some aldehydes substituted with electron-withdrawing and electron-donating groups were

Table 1. Knoevenagel reaction of aromatic aldehydes and active methylene compounds catalyzed by MNP@PEG-ImOH in aqueous medium[a]

Aldehyde	R or X	Product	Time, h	Yield,[b] %
Benzaldehyde	Me	**6a**	2.5	93
2-Chlorobenzaldehyde	Me	**6b**	3	89
3-Chlorobenzaldehyde	Me	**6c**	3	91
4-Chlorobenzaldehyde	Me	**6d**	2.5	89
4-Hydroxybenzaldehyde	Me	**6e**	3	87
3-Nitrobenzaldehyde	Me	**6f**	3	87
4-Methylbenzaldehyde	Me	**6g**	2.5	91
4-Methoxybenzaldehyde	Me	**6h**	2.5	92
4-(Dimethylamino)benzaldehyde	Me	**6i**	3.5	89
2-Furaldehyde	Me	**6j**	2	89
Benzaldehyde	H	**7a**	3	91
2-Chlorobenzaldehyde	H	**7b**	3.5	88
3-Chlorobenzaldehyde	H	**7c**	3	89
4-Chlorobenzaldehyde	H	**7d**	2.5	87
4-Hydroxybenzaldehyde	H	**7e**	3.5	87
3-Nitrobenzaldehyde	H	**7f**	3.5	88
4-Methylbenzaldehyde	H	**7g**	3	90
4-Methoxybenzaldehyde	H	**7h**	2.5	91
4-(Dimethylamino)benzaldehyde	H	**7i**	3.5	85
2-Furaldehyde	H	**7j**	2.5	86
Benzaldehyde	CN	**8a**	0.3	94, trace,[c] 45,[d] 93[e]
2-Chlorobenzaldehyde	CN	**8b**	0.5	92
3-Chlorobenzaldehyde	CN	**8c**	0.6	90
4-Chlorobenzaldehyde	CN	**8d**	0.5	89
4-Hydroxybenzaldehyde	CN	**8e**	0.75	85
3-Nitrobenzaldehyde	CN	**8f**	0.75	88
4-Methylbenzaldehyde	CN	**8g**	0.3	92
4-Methoxybenzaldehyde	CN	**8h**	0.3	91
4-(Dimethylamino)benzaldehyde	CN	**8i**	0.75	86
2-Furaldehyde	CN	**8j**	0.3	90
Benzaldehyde	COOEt	**9a**	0.5	90
2-Chlorobenzaldehyde	COOEt	**9b**	0.5	89
4-Chlorobenzaldehyde	COOEt	**9c**	0.5	91
4-Hydroxybenzaldehyde	COOEt	**9d**	0.75	88
3-Nitrobenzaldehyde	COOEt	**9e**	1	87
2-Furaldehyde	COOEt	**9f**	0.5	85

[a] Reaction conditions: aldehyde (1 mmol), active methylene compound (1 mmol), catalyst (0.02 g), water (3 mL), r.t.
[b] Isolated yield.
[c] Without a catalyst.
[d] 0.01 g of the catalyst.
[e] 0.03 g of the catalyst.

examined in the Knoevenagel condensation which afforded desired products in high yields (Table 1).

Prominent characteristics of the MNP@PEH-ImOH catalyst include the unique features of magnetic NPs and the presence of polyethylene glycol and imidazolium ring in the catalyst structure, which endows it with a PTC feature and enhances its organophilicity.

In the next step, we chose the reaction of benzaldehyde with malononitrile as a model for testing catalyst reusability. The reaction was implemented for 5 successive runs. Upon the end of each run, an external magnet was used to separate the catalyst from the reaction mixture. The catalyst was then washed with acetone or methanol and reapplied for another run. It is notable that the yields of the product remained comparable in all runs (94, 93, 90, 89, and 87% in cycles 1–5, respectively). Thus, the catalyst can be recycled for at least 5 times without a significant decrease in its activity (Fig. 7).

The energy of the frontier molecular orbitals, HOMO and LUMO, and their energy gaps for benzaldehyde (**1**), dimedone (**2**) and cyclohexane-1,3-dione (**3**) in both tautomeric forms (keto and enol) were computed at the B3LYP/Def2-TZVP level of theory. These results and the gas-phase optimized structures of compounds **1**, **2**, and **3** are shown in Fig. 8. The calculations showed that the keto forms of **2** and **3** are, respectively, 3.73 and 3.26 kcal/mol more stable than the enol forms. Thus, the enol forms are softer and more reactive than keto forms, as reflected from the energy gap values by 0.385 eV (8.88 kcal/mol) for dimedone and 0.344 eV (7.93 kcal/mol) for cyclohexane-1,3-dione.

The reaction of benzaldehyde and ethyl cyanoacetate can produce two diastereoisomeric products

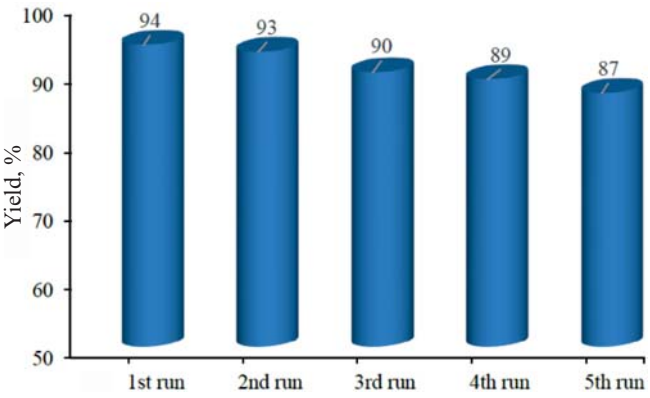

Fig. 7. Reusability of the catalyst.

(Fig. 9). In order to analyze the two isomeric structures of **9a** in greater detail, DFT calculations were carried out at the B3LYP/Def2-TZVP level of theory. As expected, the calculations showed that the *E* isomer is 4.71 kcal/mol more stable than the *Z* isomer.

In conclusion, this study dealt with the synthesis and characterization of an effective, magnetically recoverable, reusable, and thermally stable nanomagnetic supported basic ionic liquid (MNP@PEG-ImOH). The use of this magnetic nanocomposite in the Knoevenagel condensation of aromatic aldehydes with active methylene compounds in aqueous medium at room temperature offered numerous benefits, like a higher yield, more acceptable reaction conditions, shorter reaction time, reusability of the catalyst, and simplified workup.

EXPERIMENTAL

Commercially available reagents and solvents were purchased from Merck and Sigma–Aldrich. Fe_3O_4@SiO_2@PEG, Fe_3O_4@SiO_2, and Fe_3O_4 were prepared

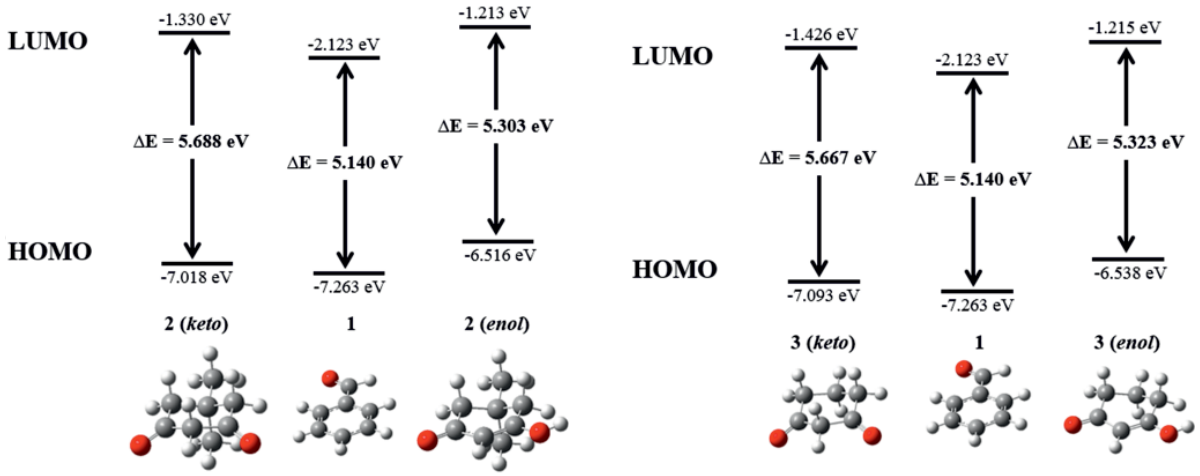

Fig. 8. HOMO and LUMO energies and energy gaps of benzaldehyde (**1**), dimedone (**2**) and cyclohexane-1,3-dione (**3**).

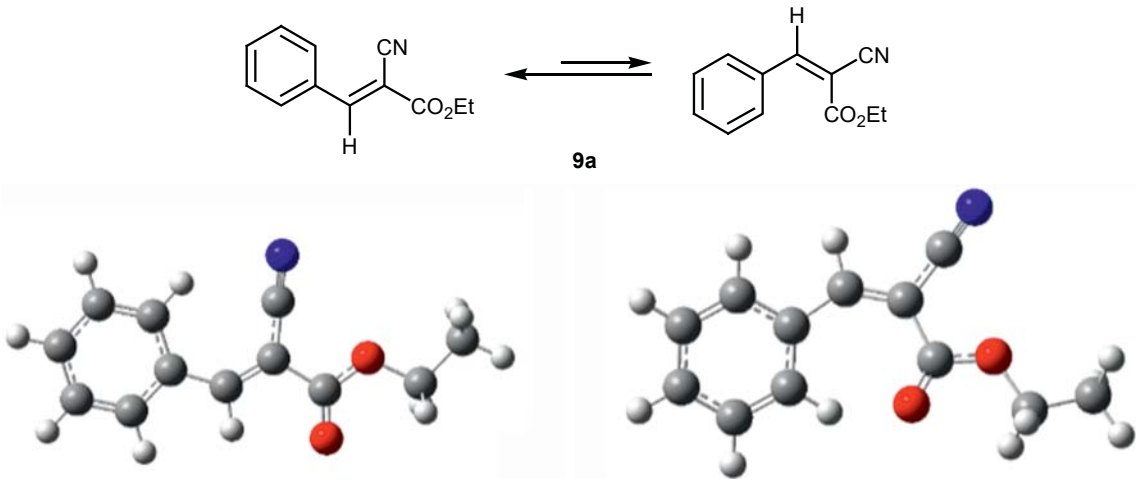

Fig. 9. Optimized structures of the *E* and *Z* isomers of compound **9a**.

according to the reported procedures [31, 33]. The progress of reactions was monitored by TLC on Polygram SILG/UV254 silica gel plates. Each product was characterized by physical data and by comparison with authentic samples; the melting points were measured in open capillary tubes using an Electrothermal 9200 apparatus. The IR spectra were registered on a Shimadzu IR Prestige-21 spectrometer in the range from 4000 to 400 cm^{-1}. The X-ray diffraction patterns were obtained with a PANalytical X'Pert Pro diffractometer. Energy-dispersive X-ray spectroscopy (EDAX) and field emission scanning electron microscopy (FESEM) were run with a Zeiss Sigma VP instrument. The TEM images of the catalyst were registered with a Zeiss-EM10C transmission electron microscope. Thermogravimetric analysis (TGA) was performed using a TA Q600 analyzer (temperature range 25 to 800°C, heating rate 10 deg/min, air atmosphere). The magnetic features of the NPs were studied with a Meghnatis Daghigh Kavir vibrating sample magnetometer (Kashan, Iran) at room temperature. Density functional theory (DFT) calculations were performed with the Gaussian 09 package at the B3LYP level of theory utilizing Def2-TZVP basis set.

Preparation of MNP@PEG-ImOH. MNP@PEG (4 g) [31] was ultrasonically dispersed in toluene (100 mL), pyridine (4 mL, 50 mmol) and thionyl chloride (6 mL, 50 mmol) were added, and the mixture was stirred under reflux for 6 h. The nanoparticles were separated by a magnet, washed with ethanol (3× 10 mL), and dried in an oven at 60°C for 12 h. Next, 1-methylimidazole (8 g, 100 mmol) was added to a suspension of MNP@PEG-Cl (4 g) in CH_2Cl_2 (60 mL), and the mixture was stirred and refluxed for 12 h. The product was separated by an external magnet, washed many times with EtOH and CH_2Cl_2, and dried in an oven at 60°C for 12 h. Finally, a mixture of sodium hydroxide (1 g, 25 mmol) and MNP@PEG-ImCl (4 g) in water (20 mL) was stirred at room temperature for 24 h. The catalyst was separated using an external magnet, washed with acetonitrile and ethanol, and thoroughly dried.

General procedure for the Knoevenagel condensation catalyzed by MNP@PEG-ImOH. The catalyst MNPs@PEG-ImOH (0.02 g) was added to a mixture of active methylene compound **2**–**5** (1 mmol) and aromatic aldehyde **1** (1 mmol) in water (3 mL). The mixture was stirred at ambient temperature for a suitable time (see Table 1). After completion of the reaction (TLC, ethyl acetate–*n*-hexane, 2:5), the mixture was filtered using a magnet to separate the catalyst. The filtrate was evaporated, and the solid product was purified by recrystallization from ethanol.

CONFLICT OF INTEREST

The authors declare the absence of conflict of interest.

REFERENCES

1. Campisciano, V., Giacalone, F., and Gruttadauria, M., *Chem. Rec*., 2017, vol. 17, p. 918. https://doi.org/10.1002/tcr.201700005
2. Rodríguez-Pérez, L., Teuma, E., Falqui, A., Gómez, M., and Serp, P., *Chem. Commun*., 2008, p. 4201. https://doi.org/10.1039/B804969F
3. Tan, J., Liu, X., Yao, N., Hu, Y.L., and Li, X.H., *ChemistrySelect*, 2019, vol. 4, p. 2475. https://doi.org/10.1002/slct.201803739

4. Polesso, B.B., Bernard, F.L., Ferrari, H.Z., Duarte, E.A., Vecchia, F.D., and Einloft, S., *Heliyon*, 2019, vol. 5, article ID e02183. https://doi.org/10.1016/j.heliyon.2019.e02183
5. Rostamizadeh, S., Zekri, N., and Tahershamsi, L., *Chem. Heterocycl. Compd*., 2015, vol. 51, p. 526. https://doi.org/10.1007/s10593-015-1728-z
6. Wang, T., Wang, W., Lyu, Y., Chen, X., Li, C., Zhang, Y., Song, X., and Ding, Y., *RSC Adv*., 2017, vol. 7, p. 2836. https://doi.org/10.1039/C6RA26780G
7. Patel, N., Katheriya, D., Dadhania, H., and Dadhania, A., *Res. Chem. Intermed*., 2019, vol. 45, p. 5595. https://doi.org/10.1007/s11164-019-03922-0
8. *Ionic Liquids: Applications and Perspectives*, Kokorin, A., Ed., Rijeka, Croatia: InTech, 2011.
9. Hu, Y.L. and Fang, D., *J. Mex. Chem. Soc*., 2017, vol. 60, p. 207. https://doi.org/10.29356/jmcs.v60i4.113
10. Tamami, B., Sardarian, A., and Ataollahi, E., *Turk. J. Chem*., 2016, vol. 40, p. 422. https://doi.org/10.3906/kim-1504-40
11. Khanapure, S., Jagadale, M., Kale, D., Gajare, S., and Rashinkar, G., *Aust. J. Chem*., 2019, vol. 72, p. 513. https://doi.org/10.1071/CH18576
12. Polshettiwar, V., Luque, R., Fihri, A., Zhu, H., Bouhrara, M., and Basset, J.-M., *Chem. Rev*., 2011, vol. 111, p. 3036. https://doi.org/10.1021/cr100230z
13. Jiang, Y., Guo, C., Xia, H., Mahmood, I., Liu, C., and Liu, H., *J. Mol. Catal. B: Enzym*., 2009, vol. 58, p. 103. https://doi.org/10.1016/j.molcatb.2008.12.001
14. Bagheri, M., Masteri-Farahani, M., and Ghorbani, M., *J. Magn. Magn. Mater*., 2013, vol. 327, p. 58. https://doi.org/10.1016/j.jmmm.2012.09.038
15. Garkoti, C., Shabir, J., and Mozumdar, S., *New J. Chem*., 2017, vol. 41, p. 9291. https://doi.org/10.1039/C6NJ03985E
16. Makosza, M., *Pure Appl. Chem*., 2000, vol. 72, p. 1399. https://doi.org/10.1351/pac200072071399
17. Davarpanah, J. and Kiasat, A.R., *Catal. Commun*., 2013, vol. 42, p. 98. https://doi.org/10.1016/j.catcom.2013.07.040
18. Ayashi, N., Fallah-Mehrjardi, M., and Kiasat, A.R., *Russ. J. Org. Chem*., 2017, vol. 53, p. 846. https://doi.org/10.1134/S1070428017060069
19. Jain, Y., Kumari, M., Agarwal, M., and Gupta, R., *Carbohydr. Res*., 2019, vol. 482, article ID 107736. https://doi.org/10.1016/j.carres.2019.06.015
20. Rezvani, M.A., Oghoulbeyk, Z.N., Khandan, S., and Mazzei, H.G., *Polyhedron*, 2020, vol. 177, article ID 114291. https://doi.org/10.1016/j.poly.2019.114291
21. Mase, N. and Horibe, T., *Org. Lett*., 2013, vol. 15, p. 1854. https://doi.org/10.1021/ol400462d
22. Poor Heravi, M.R. and Piri, S., *J. Chem*., 2013, vol. 2013, article ID 652805. https://doi.org/10.1155/2013/652805
23. Ogiwara, Y., Takahashi, K., Kitazawa, T., and Sakai, N., *J. Org. Chem*., 2015, vol. 80, p. 3101. https://doi.org/10.1021/acs.joc.5b00011
24. van Schijndel, J., Canalle, L.A., Molendijk, D., and Meuldijk, J., *Green Chem. Lett. Rev*., 2017, vol. 10, p. 404. https://doi.org/10.1080/17518253.2017.1391881
25. Kakesh, N., Sayyahi, S., and Badri, R., *C. R. Chim*., 2018, vol. 21, p. 1023. https://doi.org/10.1016/j.crci.2018.09.009
26. Shaterian, H.R., Arman, M., and Rigi, F., *J. Mol. Liq*., 2011, vol. 158, p. 145. https://doi.org/10.1016/j.molliq.2010.11.010
27. Mochalov, S.S., Chasanov, M.I., Fedotov, A.N., and Zefirov, N.S., *Chem. Heterocycl. Compd*., 2011, vol. 47, p. 1105. https://doi.org/10.1007/s10593-011-0881-2
28. Kühbeck, D., Saidulu, G., Reddy, K.R., and Díaz, D.D., *Green Chem*., 2012, vol. 14, p. 378. https://doi.org/10.1039/C1GC15925A
29. Levchenko, K.S., Chudov, K.A., Zinoviev, E.V., Lyssenko, K.A., Fakhrutdinov, A.N., Demin, D.U., Poroshin, N.O., Shmelin, P.S., and Grebennikov, E.P., *Tetrahedron Lett*., 2019, vol. 60, p. 1505. https://doi.org/10.1016/j.tetlet.2019.04.050
30. Tarade, K., Shinde, S., Sakate, S., and Rode, C., *Catal. Commun*., 2019, vol. 124, p. 81. https://doi.org/10.1016/j.catcom.2019.03.005
31. Kiasat, A.R. and Davarpanah, J., *J. Mol. Catal. A: Chem*., 2013, vol. 373, p. 46. https://doi.org/10.1016/j.molcata.2013.03.003
32. Amini, A., Sayyahi, S., Saghanezhad, S.J., and Taheri, N., *Catal. Commun*., 2016, vol. 78, p. 11. https://doi.org/10.1016/j.catcom.2016.01.036
33. Kassaee, M.Z., Masrouri, H., and Movahedi, F., *Appl. Catal., A*, 2011, vol. 395, p. 28. https://doi.org/10.1016/j.apcata.2011.01.018